Quaternary Science Reviews 239 (2020) 106356

Contents lists available at ScienceDirect

Quaternary Science Reviews

journal homepage: www.elsevier.com/locate/quascirev

Late pleistocene paleoceanographic changes in the Ross Sea – Glacial-interglacial variations in paleoproductivity, nutrient utilization, and deep-water formation

Sunghan Kim [a, *], Jae Il Lee [a], Robert M. McKay [b], Kyu-Cheul Yoo [a], Young-Suk Bak [c], Min Kyung Lee [a], Youn Ho Roh [a, d], Ho Il Yoon [a], Heung Soo Moon [a], Chang-Uk Hyun [a]

[a] Korea Polar Research Institute, Incheon, 21990, South Korea
[b] Antarctic Research Centre, Victoria University of Wellington, Wellington, 6140, New Zealand
[c] Department of Earth and Environmental Sciences, Chonbuk National University, Jeonju, 54896, South Korea
[d] University of Science and Technology, Daejeon, 34113, South Korea

ARTICLE INFO

Article history:
Received 12 April 2020
Accepted 1 May 2020
Available online xxx

Keywords:
Ross sea
Antarctic slope current
Pleistocene
Paleoproductivity
Nutrient utilization
Carbonate
Deep-water formation

ABSTRACT

The outer Ross Sea continental shelf has experienced large variations in ice sheet extent over the Pleistocene that are theorized to be largely driven by changes in the westward-flowing Antarctic Slope Current (ASC) at the continental shelf break. This current regulates southward incursions of warm modified Circumpolar Water, and it is thought to have triggered past marine ice sheet retreat. Additionally, expansions of grounded ice sheets on the continental shelf have fundamentally altered the Ross Sea water mass formation processes, influencing surface water salinity, sea ice cover, nutrient utilization, deep-water ventilation, and primary productivity. Here, we report the geochemical, physical properties, grain size, bulk $\delta^{15}N$, and diatom records during the late Pleistocene from two sediment cores from the Iselin Bank on the outermost continental shelf in the Ross Sea. These core sites were not overridden by grounded ice sheets during the late Pleistocene glacial-interglacial cycles, allowing for a continuous archive of glacimarine environments that were influenced by the ASC. Interglacial periods are typically characterized by high surface water productivity and nutrient utilization, with *Chaetoceros* resting spores indicating nutrient limitation under open ocean conditions, and glacial periods are typically characterized by low surface water productivity and nutrient utilization, with sea ice diatoms and planktonic foraminifers indicating light limitation under extensive sea ice/ice margin proximal conditions. A grain size analysis indicates coarse-skewed distributions and winnowing in the Iselin Bank region during cold periods. The winnowing may be related to enhanced ASC flow instead of density driven shelf water outflow.

1. Introduction

The modern Ross Sea is characterized by the Ross Ice Shelf which is fed by ice from both the East Antarctic Ice Sheet (EAIS) and West Antarctic Ice Sheet (WAIS). During past glacial expansions these ice masses were grounded over much of the outer continental shelf edge in the Ross Sea (Anderson et al., 2014). The ANDRILL AND-1B cores collected beneath the Ross Ice Shelf showed that changes in Ross Sea shelf sedimentary facies correspond to up to 28 expansion and retreat cycles between 5 and 1 Ma, but they contained numerous hiatuses due to periods of glacial erosion (Naish et al., 2009). However, although the evidence for WAIS collapse after 1 Ma remains equivocal, the sedimental facies and deformational features of AND-1B suggest that shifts between grounded ice sheet and floating ice shelf conditions have occurred in the past 1 Ma at frequencies consistent with those of orbital pacing (McKay et al., 2012). Although the exact timing of these events in AND-1B remains difficult to constrain, seismic surveys in the Northern Basin of the Ross Sea also indicate that there were shelf-wide advancements and retreats during the Plio-Pleistocene (Bart et al., 2011; Anderson et al., 2019). Given that the Ross Sea experienced large shifts in ice sheet coverage during the Plio-Pleistocene ice age cycles and is currently a key area for Antarctic Bottom Water (AABW) formation and sea ice production (Smith

* Corresponding author.
E-mail address: delongksh@kopri.re.kr (S. Kim).

https://doi.org/10.1016/j.quascirev.2020.106356

et al., 2012), the outer continental shelf in the Ross Sea is an ideal region for investigating oceanic changes through past glacial-interglacial changes.

The last four glacial-interglacial cycles are characterized by large glacial-interglacial variations in ice volume, temperature, sea-level, and pCO_2 (Bintanja et al., 2005; Lisiecki and Raymo, 2005; Jouzel et al., 2007; Lüthi et al., 2008; Siddall et al., 2010). However, Ross Shelf sediment records are largely restricted to the last glacial period due to difficulties in obtaining sediment cores that can penetrate the Last Glacial Maximum glacial sediments (e.g., Cunningham et al., 1999; Domack et al., 1999; Licht et al., 1999; Anderson et al., 2014; McKay et al., 2016), and more continuous sedimentary records from Ross Sea continental slope/rise are sparse (e.g., Ceccarori et al., 1998). Although five sites at the Ross Sea shelf and slope were drilled during International Ocean Discovery Program Expedition 374 in 2018 (McKay et al., 2019), the detailed scientific analyses are ongoing. Thus, a large gap remains in our understanding of ice shelf and ice sheet changes and their oceanic impacts on the Ross Sea during the late Pleistocene. Furthermore, it is undetermined whether changes in the Ross Sea are synchronous with those in other Antarctic regions, the Southern Ocean (Hillenbrand et al., 2009), and global paleoceanographic records on AABW formation (Hodell and Venz-Curtis, 2006; Elderfield et al., 2012).

Sedimentary facies on the Antarctic continental shelf, including the Ross Sea, are commonly associated with the position of the ice shelf grounding and calving line, but they can also be influenced by the meltwater or mass flow processes (e.g., Domack et al., 1999; McKay et al., 2009, 2012; McGlannan et al., 2017; Simkins et al., 2017; Prothro et al., 2018). Although sediment trap studies in the Ross Sea showed significant fluxes in $CaCO_3$ toward the seafloor (Collier et al., 2000), sediment cores containing $CaCO_3$ in the Ross Sea are extremely limited due to their poor preservation of corrosive bottom water mass (Kennett, 1968; Anderson, 1975; Anderson et al., 2014). Some sediment cores in the outer shelf regions with Circumpolar Deep Water (CDW) influence exhibit high $CaCO_3$ concentrations, but the major constituents are benthic carbonates (e.g., Taviani et al., 1993; Licht et al., 1996; Frank et al., 2014). Due to the limited number of studies on $CaCO_3$ enriched deposits in this setting, there is a lack understanding of 1) the dynamics of surface water $CaCO_3$ changes through time despite significant production in modern surface water and 2) how shifting bottom water properties over time may influence carbonate preservation.

In this study, we developed a multi-proxy record using geochemical (biogenic opal, $CaCO_3$, and total organic carbon (TOC) concentrations), bulk $\delta^{15}N$, physical properties (magnetic susceptibility (MS), water content (WC), and grain density), grain size, and diatom assemblages from two sediment cores in the outermost Ross Sea. These multiproxy records allow for the novel reconstruction of glacial-interglacial changes in surface water productivity, nutrient utilization, current speed, ice rafting, and bottom water mass during the last four glacial-interglacial cycles. We also infer how these paleooceanographic changes may relate to changes in ice sheet and ice shelf coverage on the Ross Sea continental shelf during this time period.

2. Study area

The Iselin Bank is a submarine bank located in the northern edge of the Ross Sea continental shelf break (Fig. 1), and it was not covered by a grounded ice sheet during the last glacial period (Anderson et al., 2002; Bentley et al., 2014). Because the Iselin Bank forms a bathymetric high, the bottom water/current in the shelf region flows into adjacent troughs (Dinniman et al., 2011; Smith et al., 2012), and the sedimentation in this region is therefore not significantly influenced by density currents. However, the Iselin Bank is located in the path of Antarctic Slope Current (ASC) which flows westward along the continental slope (Smith et al., 2012). The ASC is characterized by a subsurface front that separates Antarctic Surface Water on the shelf from the CDW on the lower continental slope (Orsi and Wiederwohl, 2009). Because this front serves as a barrier to prevent the transfer of CDW to the Ross Sea continental shelf (Ainley and Jacobs, 1981; Thompson et al., 2018), ASC vigor may have regulated the intrusion of CDW into the Ross Sea continental shelf and influenced the marine ice sheet variance over past Plio-Pleistocene glacial-interglacial (Naish et al., 2009). Because of the Iselin Bank's relatively shallower water depths, $CaCO_3$ is better preserved in sediments in the Iselin Bank than in deeper water continental slope/rise; however, it is more likely to contain a complete record than that of the glacially-eroded Ross Sea continental shelf. Nevertheless, no detailed sedimentary studies of late Pleistocene records have been conducted from the Iselin Bank.

Although the sea ice coverage in the Ross Sea exhibits large annual variations, an open water polynya typically forms across much of the Ross Sea from December to February (NSIDC, 1998). The average surface chlorophyll and carbon concentrations of the Ross Sea water column are high between November and March, when the seasonal sea ice retreats (Arrigo and van Dijken, 2004). However, major surge of biogenic opal export occurs during the fall sea ice regrowth phase (Collier et al., 2000). The mismatch in surface water production observed in satellite data versus sediment traps is likely the consequence of recycling of phytoplankton blooms in the upper Ross Sea-water column (Collier et al., 2000).

3. Materials and methods

Two sediment cores were collected from the western flank of the Iselin Bank by the IBR/V *Araon* during the ANA05B cruise in 2015, the 2.57-m-long RS15-GC40 (71°37.0044′S, 178°17.4630′W, 1083 m in depth) and the 5.4-m-long RS15-GC41 (71°23.0785′S, 178°59.2588′W, 1557 m in depth). Both gravity cores were opened, described, sampled, and analyzed at the Korea Polar Research Institute (KOPRI), South Korea.

3.1. Physical properties (MS, WC, and grain density)

The MS of the two cores was measured at 1-cm intervals on split half-core sections using a Bartington MS-2B susceptibility meter. Before splitting the core sections, whole-round MS values were measured at 1-cm intervals using a core logging sensor (Bartington MS2C). The WC of the two cores was measured at 1-cm intervals on 1-cm-thick sub-samples and was calculated using the following equation with an assumption of 35 psμ for seawater:

WC (%) = (mass of wet sediment − (mass of dry sediment + mass of salt))/mass of wet sediment × 100.

The grain density was measured at 2 cm intervals for RS15-GC40 and 5 cm intervals for RS15-GC41 on 1 cm thick sub-samples using a gas pycnometer (AccuPyc II 1340).

3.2. Geochemical proxies (biogenic opal, TOC, and $CaCO_3$ concentrations)

Geochemical proxies for the two cores were measured from 1-cm-thick samples collected at 5-cm intervals. Biogenic silica (Si_{BIO}) concentrations were measured using a continuous flow analyzer (SKALAR SAN^{plus} Analyzer) and the wet-alkaline extraction method modified from DeMaster (1981) at the KOPRI (Kim et al., 2018). Biogenic opal concentrations were calculated by multiplying biogenic silica concentrations by 2.4, the ratio of

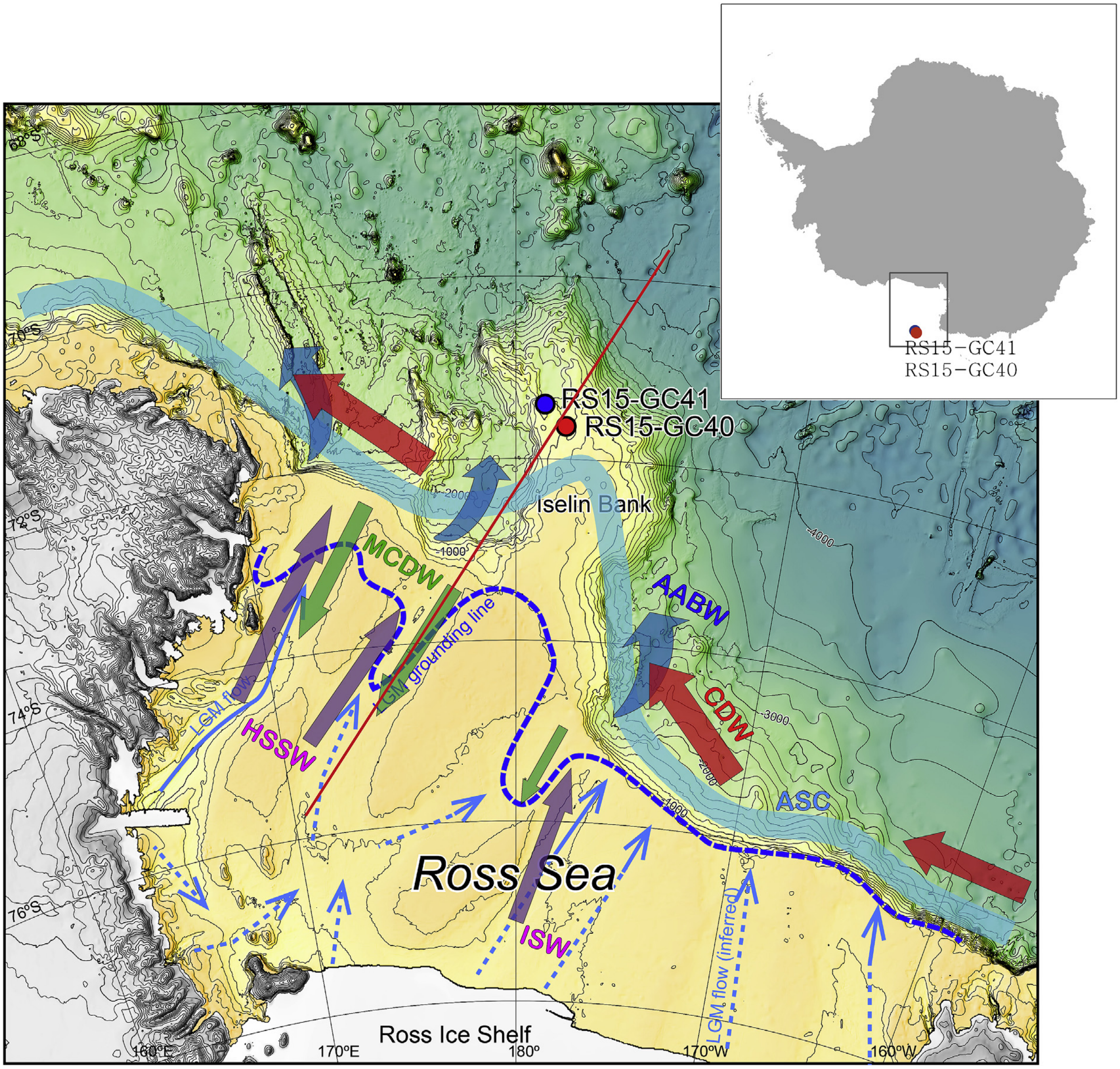

Fig. 1. Regional map of the Ross Sea showing core locations of RS15-GC40 and RS15-GC41. Last Glacial Maximum (LGM) grounding line (blue dashed) and LGM ice flow directions (sky blue arrows) are modified from Anderson et al. (2002). Antarctic Slope Current (ASC), Antarctic Bottom Water (AABW), Circumpolar Deep Water (CDW), Modified CDW (MCDW), High Salinity Shelf Water (HSSW), and Ice Shelf Water (ISW) are modified from Smith et al. (2012). The red line is the axis for schematic model Fig. 6.

biogenic opal (SiO_2+nH_2O)/Si that was determined by assuming that nH_2O constitutes 10% of biogenic SiO_2 (Mortlock and Froelich, 1989). The relative analytical error of biogenic silica concentration in sediment samples is less than 1%. Total inorganic carbon (TIC) concentration was measured using UIC CO_2 coulometer (Model CM5240) at the KOPRI. $CaCO_3$ concentrations were calculated by multiplying TIC concentrations by 8.333, the ratio of $CaCO_3$/C. The relative standard deviation for $CaCO_3$ concentration is ±1%. Total carbon (TC) concentration was measured using an organic elemental analyzer (FLASH, 2000 NC Analyzer) with an analytical precision of less than ±0.1%. TOC concentrations were calculated as the difference between TC and TIC.

3.3. Bulk $\delta^{15}N$ values

Bulk $\delta^{15}N$ values for the two cores were measured at 5-cm intervals using Europa Scientific RoboPrep-CN elemental analyzer and Europa Scientific 20-20 isotopic ratio mass spectrometer from Iso-Analytical Ltd., UK. Nitrogen isotope ratios were expressed in the conventional delta notation, which is the per mil deviation from atmospheric nitrogen. The precision for nitrogen isotopes was approximately ±0.2‰.

3.4. Grain size analysis

After removing the organic matter and biogenic silica from the bulk sediments using 10% H_2O_2 and 2N NaOH, respectively, grain size was analyzed at-4 cm intervals for the two cores. Coarser fractions (>63 μm) were weighed at 1-phi intervals using sieves, while finer fractions (<63 μm) were analyzed using a Micrometrics Sedigraph III 5120 at the KOPRI. The classification of sediments follows that of Folk and Ward (1957).

Table 1
Radiocarbon dates from RS15-GC40 and RS15-GC41. The calibration program CALIB 7.1 (Stuiver and Reimer, 1993; Reimer et al., 2013) was used to convert the ^{14}C ages to calendar ages (σ2) with a reservoir correction of 1300 years (△R = 900 years). BF: benthic foraminifer and PF: planktonic foraminifer.

Depth (cm)	Analyzed material	Lab code	^{14}C age (yr BP)	Error (yr)	$\delta^{18}O$ (‰)	cal. yr BP (min)	cal. yr BP (max)	Calendar age (yr BP)
RS15-GC40								
3	BF + PF	Rafter-40933/1	17,432	±79	–	19,212	19,685	19,460
5	PF	Beta-489,452	21,790	±70	+4.7	24,360	24,978	24,642
30	PF	Beta-489,453	43,290	±620	+4.4	44,228	46,462	45,329
100	BF + PF	Rafter-40933/2	Back-ground					
RS15-GC41								
23	BF + PF	Rafter-40933/3	17,791	±86	–	19,620	20,125	19,887
25	PF	Beta-489,454	18,760	±60	+5.1	20,850	21,317	21,073

3.5. Diatom assemblage analysis

Thirty-two diatom assemblage samples for RS15-GC41 containing either a high or low biogenic opal concentration were analyzed at approximately 15-cm intervals. Due to the low abundances in many samples, up to 200 diatom specimens were counted. For samples with extremely low diatom abundances, 200 microscope fields of view were observed and counted. The sample preparation and diatom counting methods followed those described in Bak et al. (2007). The quantitative analysis of the diatom slides followed the procedures described in Scherer (1994). Absolute abundance was calculated using the following equation: abundance = ((A × B)/(C × D))/E, where A is the number of specimens counted, B is the area of the settling chamber, C is the number of microscope fields of view, D is the area of the field of view, and E is the sample mass. *Chaetoceros* resting spores were not included in the specimen count.

3.6. Radiocarbon dating

Accelerator mass spectrometry (AMS) ^{14}C dates were either measured using the planktonic foraminifer *Neogloboqudria pachyderma* (sin.) or using a mixture of planktonic and benthic foraminifers. Four intervals in RS15-GC40 and two intervals in RS15-GC41 were dated at Beta Analytic, USA or Rafter Radiocarbon, New Zealand (Table 1). Beta Analytic also provided the $\delta^{18}O$ values of the carbonate materials (Fig. 2).

4. Age model

The radiocarbon age results were calibrated using CALIB 7.1 (Stuiver and Reimer, 1993) and the MARINE dataset (Reimer et al., 2013). Although there is a large variation in ΔR from 480 yr to 990 yr in the Antarctic regions (e.g, Domack, 1992; Domack et al., 2001; Wu et al., 2017; Christ et al., 2015; Hillenbrand et al., 2010; Kim et al., 2018), we used a ΔR of 900 years. Regardless of which reservoir ages are used, the chronological framework for the two cores is nearly the same considering the time scales for the two cores. We used planktonic foraminifer AMS ^{14}C dates as the tie points for the uppermost sediments which constrain the timing of the Last Glacial Maximum to 26.5 ka to 19 ka (Clark et al., 2009) for both cores (Fig. 2). The ages of 19.5 ka at 3 cm and 24.5 ka at 5 cm in

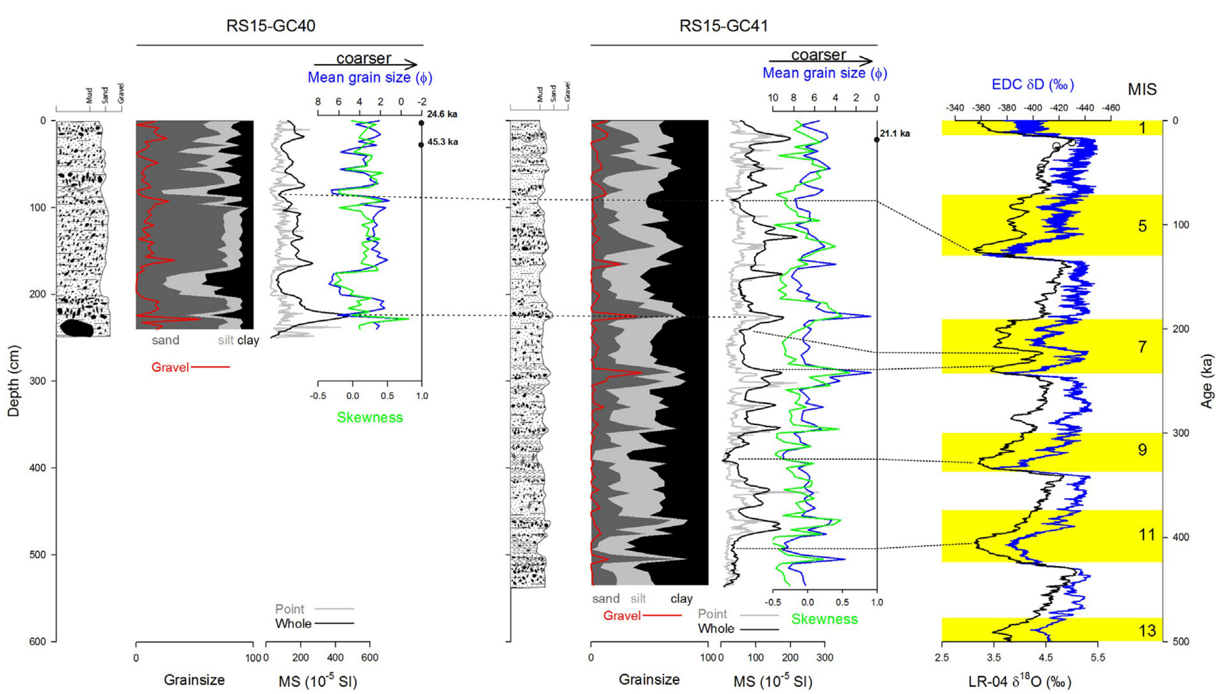

Fig. 2. Graphical correlations of MS values between RS15-GC40 and RS15-GC41 and graphical correlations of MS values of RS15-GC41 with LR-04 $\delta^{18}O$ (Lisiecki and Raymo, 2005) and EDC δD and dust record (Jouzel et al., 2007). Interglacial periods are marked by yellow box with marine isotope stage (MIS) numbers. Lithofacies, skewness, mean grain size, and grain size, normalized to sand/silt/clay total, of two cores are plotted together. Black closed circles are foraminifer AMS ^{14}C dates and their **$\delta^{18}O$ values (open circles)** are plotted together with LR-04 $\delta^{18}O$.

Table 2
Tie points obtained by whole round measured MS graphical correlations between RS15-GC40 and RS15-GC41 and tie points obtained by graphical correlations of RS15-GC41 whole round measured MS and LR-04 (Lisiecki and Raymo, 2005).

RS15-GC40 MS to RS15-GC41 MS		RS15-GC41 MS to LR-04	
RS15-GC40 (cm)	RS15-GC41 (cm)	RS15-GC41 (cm)	LR-04 (ka)
85	91	91	126
224	227	241	222
		283	237
		387	326
		490	403

RS15-GC40 (Table 1) may be related to potential disturbance of the core top during the coring process and suggests potential core top loss, particularly for the Holocene section of RS15-GC40. The $\delta^{18}O$ values of planktonic foraminifers used for age dating correspond to the LR-04 variations (Fig. 2), and the planktonic foraminifer AMS ^{14}C ages appear to be reliable.

Because of the lack of continuous $\delta^{18}O$ stratigraphy in the Southern Ocean, previous studies covering the late Quaternary in Antarctica have constrained ages by using correlations between surface water productivity proxies such as biogenic opal/silica and Ba concentration, either measured directly or scanned using X-ray fluorescence, with an assumption that surface water productivity is high during warm periods with less sea ice (e.g., Ceccarori et al., 1998; Hillenbrand et al., 2009; Wu et al., 2017). The MS is typically negatively correlated with biogenic components in Southern Ocean sediments (e.g., Ceccarori et al., 1998; Hillenbrand et al., 2009; Yoon et al., 2009; Sprenk et al., 2013). RS15-GC40 and RS15-GC41 also demonstrate negative correlations with biogenic components (Fig. S1). As a result, high MS values typically occur during glacial periods (e.g., Ceccarori et al., 1998; Hillenbrand et al., 2009). Therefore, we graphically correlate whole-round MS values with the LR04 $\delta^{18}O$ stack using Analyseries software (Paillard et al., 1996) (Fig. 2 and Table 2). As gravel-sized grains are dispersed randomly throughout the two cores, whole-round MS values are thought to be more representative of the bulk sediment than point MS values which can be biased toward single large grains. Although the LR04 $\delta^{18}O$ stack does not directly reflect Antarctic climate changes, the variation pattern is nearly identical to that of the EPICA Dome C (EDC) ice core δD record (Jouzel et al., 2007) (Fig. 2). The age model tie points are not a unique solution, and the visual tuning approach broad minima ties in MS occurr approximately every 1.2 m to the last four full interglacial periods in the LR04 stack and in the δD record from the EDC ice core (Fig. 2). We minimize the number of these ties and focus our interpretations of these cores on the differences in oceanographic conditions between the last four glacial-interglacial cycles since marine isotope stage (MIS) 11. The assumption that a high MS corresponds to glacial periods is further assessed, though comparisons to geochemical proxies and diatom assemblages (Figs. 3 and 4).

5. Results

The MS values of RS15-GC40 and RS15-GC41 are generally high (>100 10^{-5} SI) during glacial periods and low (<100 10^{-5} SI) during interglacial periods (Fig. 3). In contrast, WC, biogenic opal, and TOC concentrations display the opposite pattern, with high values during interglacial periods and low values during glacial periods (Fig. 3). Interglacial biogenic opal concentration peaks gradually decrease after MIS 11 in both cores (Fig. 3). TOC concentrations are generally lower than 0.2%, except for those in the core top (Fig. 3). MS values are higher for RS15-GC40 than RS15-GC41 (Fig. 3), and they display an inverse relationship with WC, suggesting that grain size (and the associated porosity) is a primary control on MS values. This inference is supported the sand percent values, where high sand percentages are related to higher MS values (Fig. 2). $CaCO_3$ concentration at the two cores is generally low (or absent) during interglacial periods and high (>5%) during glacial periods (Fig. 3). RS15-GC41 exhibits sparse $CaCO_3$ peaks at 21 ka, 298 ka, 342 ka,

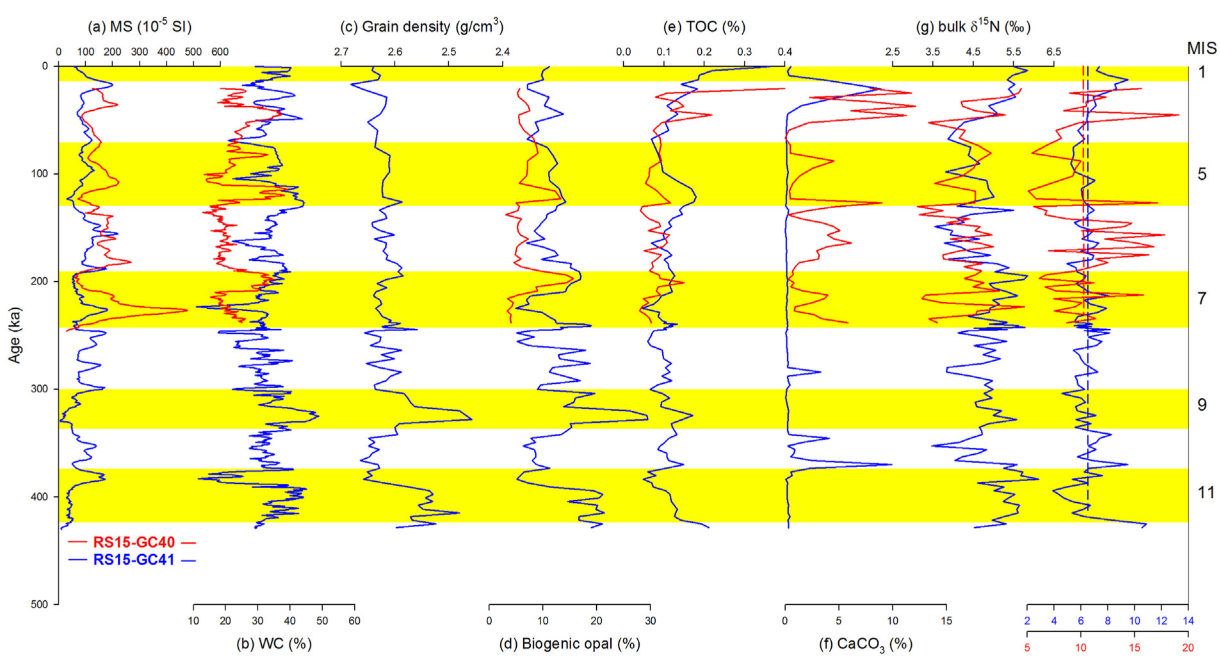

Fig. 3. Downcore profiles of (a) MS, (b) WC, (c) grain density, (d) biogenic opal concentration, (e) TOC concentration, (f) $CaCO_3$ concentration, (g) bulk $\delta^{15}N$, and (h) C/N ratio of RS15-GC40 (red) and RS15-GC41 (blue). Interglacial periods are marked by yellow box with marine isotope stage (MIS) numbers. Dashed vertical lines are mean C/N value for each core.

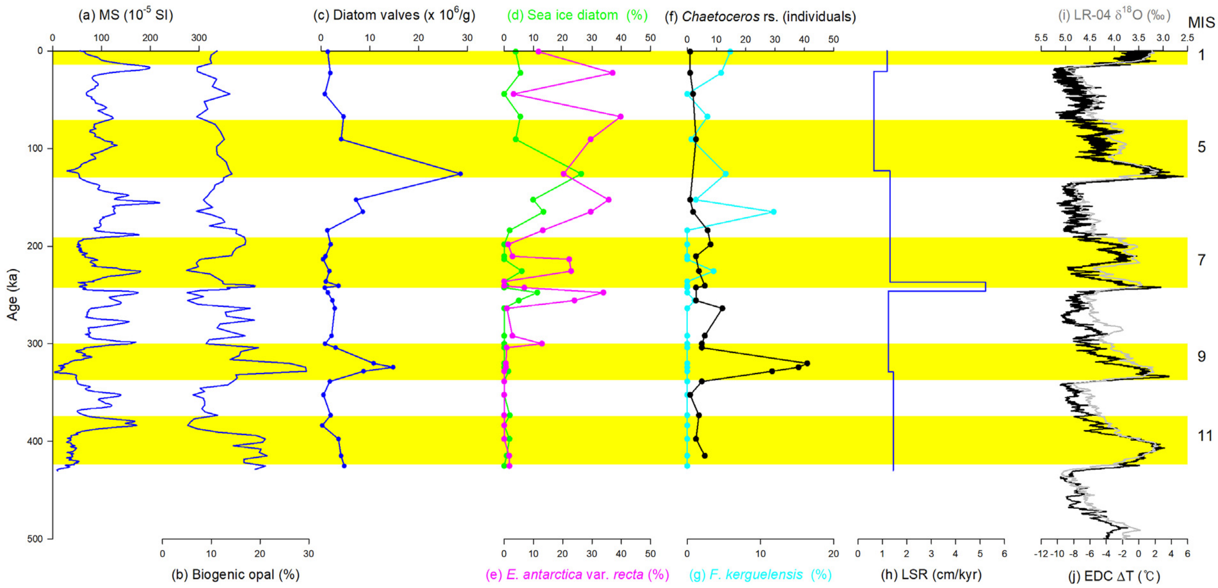

Fig. 4. Downcore profiles of (a) MS, (b) biogenic opal concentration, (c) total diatom valve, relative abundance of (d) sea ice diatoms, (e) *E. antarctica* var. *recta*, and (f) *F. kerguelensis*, (g) *Chaetoceros* resting spores, and (h) LSR of RS15-GC41 with (i) LR-04 δ^{18}O (gray, Lisiecki and Raymo, 2005), and (j) ΔT of EDC ice core (black, Jouzel et al., 2007). Interglacial periods are marked by yellow box with marine isotope stage (MIS) numbers.

and 363 ka, whereas RS15-GC40 shows broader and more frequent $CaCO_3$ peaks during glacial periods and some interglacial intervals with low biogenic opal concentrations (Fig. 3). The total diatom valve abundance of RS15-GC41 is inconsistent with biogenic opal concentration (Fig. 3). The diatom preservation status was generally poor, and the sea ice diatoms *Fragilariopsis curta* and *F. cylindrus* (Sjunneskog and Taylor, 2002; Armand et al., 2005) were not observed. However, other Antarctic sea ice related diatoms, *F. ritscheri*, *Actinocyclus actinochilus*, and *F. sublinearis* (Armand et al., 2005), were observed for RS15-GC41. In general, these sea ice diatoms were rare during high biogenic opal and TOC intervals, but were abundant during low biogenic opal and TOC intervals, and they are associated with a concomitant increase in *Eucampia antarctica* var. *recta*, a cold-water species (Leventer et al., 2002) (Fig. 4). Sea ice-related species and *E. antarctica* var. *recta* occur in higher abundances following MIS 8 (Fig. 4). The abundances of *Chaetoceros* resting spores vary and are typically low, and they are only found during intervals of high biogenic opal and TOC (Fig. 4). *F. kerguelensis* is typically absent until MIS 7 and begins to appear more abundantly during interglacial periods (Fig. 4).

RS15-GC40 is characterized by a coarser mean grain size (MGS) than that of RS15-GC41 due to its greater abundance of coarse grains (sand and gravel) (Fig. 2). The high gravel and sand contents in both cores coincide with high MS values, coarser MGSs, and coarse-skewed grain size distributions, whereas the mud content increases with lower MS intervals characterized by high biogenic opal and TOC concentrations (Figs. 2 and 3).

Bulk δ^{15}N values of the two cores vary from 3‰ to 6‰ (Fig. 3). Bulk δ^{15}N values increased during interglacial periods, particularly for high biogenic opal and TOC concentration intervals (Fig. 3). In contrast, the C/N ratios of the two cores demonstrated the opposite pattern; they were low during interglacial periods and high during glacial periods, although the C/N ratio of RS15-GC40 is higher than that of RS15-GC41 (Fig. 3).

Variations in biogenic opal, TOC, and $CaCO_3$ MARs are similar to the variations in their concentrations (Figs. 3 and 4). LSRs are high during interglacial periods and low during glacial periods. The highest LSRs occur during intervals of high biogenic opal and TOC concentrations (Figs. 3 and 4).

6. Discussion

RS15-GC40 is mainly composed of clast-rich muddy sand with well-preserved planktonic foraminifers and gradational lower contacts passing into diatom-bearing mud. RS15-GC41 is composed of interbedded clast-common/rich sandy mud to muddy sand and diatom-bearing mud. We interpret that both sites experienced alternations between interglacial open marine (diatom-bearing mud) and glacial ice proximal/extensive sea ice conditions with ice-rafting (clast-rich/common sandy mud to muddy sand). However, although these gravel grains were likely delivered by icebergs, increases in gravel are unlikely to directly relate to the dynamic ice processes, as the coarser grain concentrations may result from the winnowing processes. The occurrence of winnowing is supported by low proportions of very fine sand to coarse grains (>63 μm) (Fig. 5). The co-variation in MS and grain size indicates that the MS variation is primarily controlled by grain size, which likely relates to the presence of mafic lithologies in the sand fraction (Fig. 2). Because coarse-skewed grain size distributions in the Ross Sea outer shelf indicates the winnowing of fine materials (Prothro et al., 2018), increased skewness during intervals of high MS and gravel concentrations in the two cores indicates stronger bottom currents during glacial periods that winnowed or prevented the settling of finer-grained material at the site (Fig. 2). Despite these stronger currents, the glacial intervals of the two cores are characterized by depositions of well-preserved planktonic foraminifers, sea ice related diatoms, and *E. antarctica* var. *recta*. Consequently, the two core records are considered to reflect both surface and bottom paleoceanographic changes in the Ross Sea over the last 400 kyrs. However, increased skewness is found within the interglacial periods, such as MIS 11, 7, and 5, implying that the Ross Sea paleoceanographic changes are controlled by not only 100-kyr cycles but also by shorter 41-kyr cycles.

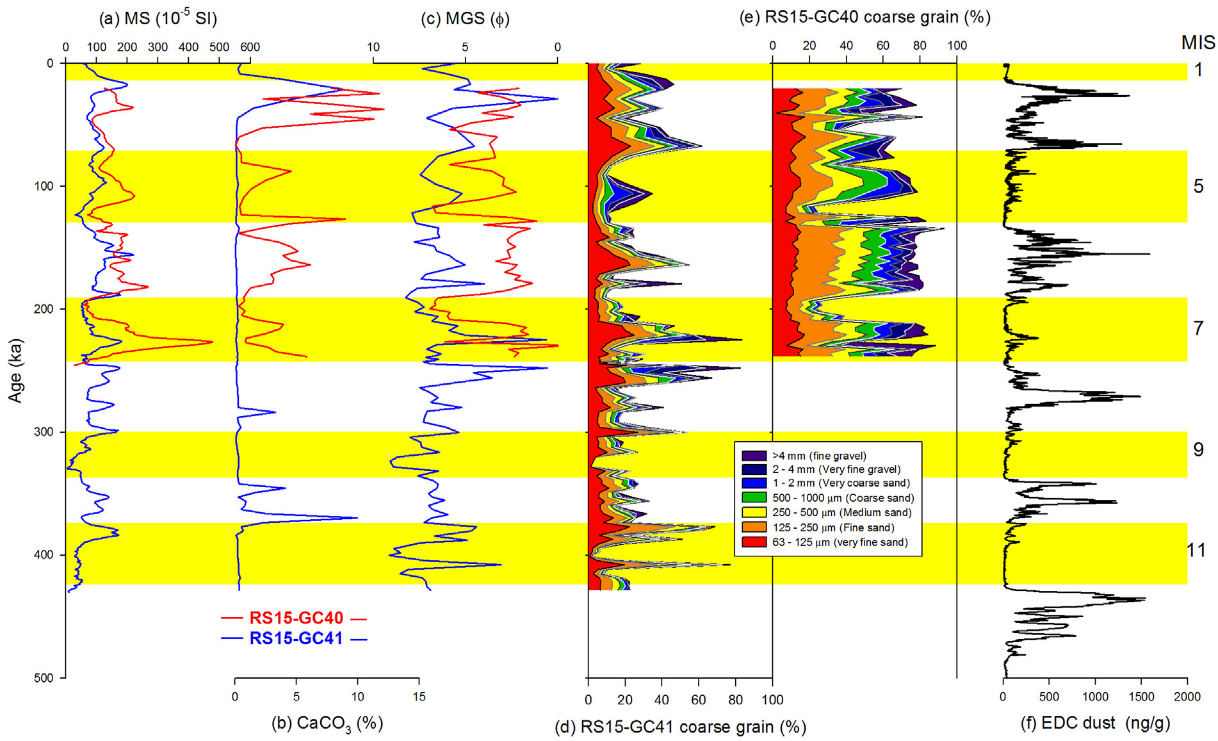

Fig. 5. Downcore profiles of (a) MS, (b) $CaCO_3$ concentration, and (c) MGS of RS15-GC40 (red) and RS15-GC41 (blue), (d) composition of coarse grains (>63 μm) of RS15-GC41 and (e) RS15-GC40 with (f) EDC ice core dust record (black, Jouzel et al., 2007).

6.1. Glacial-interglacial surface water productivity changes and associated nutrient utilization changes

The co-variations of biogenic opal and TOC at the two core sites suggest that TOC is mainly controlled by surface water diatom production (Fig. 3 and S1). Thus, lower C/N ratios during interglacial periods indicate that high biogenic opal and TOC concentrations during interglacial periods are related to increased surface water productivity in the study area because marine organic matter has a lower C/N ratio than that of terrestrial organic matter (Lamb et al., 2006 and references therein). Although terrestrial organic matter is likely to be very low in the Antarctic, the Ross Sea sediment trap record (Mooring MS-6) exhibited a seasonally lower C/N ratio during the open ocean period than that during the sea ice covered period (Collier et al., 2000), implying that a low C/N ratio is attributed to marine organic matter. In Antarctic shelf regions, surface water productivity increases as the ice shelf/sea ice retreats, particularly under open ocean conditions (Leventer and Dunbar, 1988; Cunningham et al., 1999; Domack et al., 1999; Collier et al., 2000; McKay et al., 2008; Naish et al., 2009; Prothro et al., 2018). A low MS and grain density, fine MGS, and high WC are exhibited during interglacial periods (Fig. 3), with low MS values being the consequence of increasing biogenic inputs and increased mud content. Biogenic components have lower densities than those of lithic grains, and WC increases with an increase in mud content and/or biogenic opal concentration in the sediment (e.g., Domack et al., 1999; McKay et al., 2016, Fig. S1). Thus, the characteristics of physical properties during interglacial periods imply that higher surface water productivity occurred under more open ocean conditions in the Iselin Bank region. Although decreased current speed can increase settling of biogenic material, an open ocean during interglacial periods is also supported by the increased relative abundance of the open ocean diatom species *F. kerguelensis* (Crosta et al., 2005) (Fig. 4).

Bulk $\delta^{15}N$ values in the two cores and surface water production increased during interglacial periods (Fig. 4). Because bulk $\delta^{15}N$ is used as a nutrient utilization proxy, increased $\delta^{15}N$ values indicate enhanced nitrate utilization in the Ross Sea during interglacial periods due to increased surface water production (e.g., Robinson et al., 2014; Kim et al., 2018 and references therein). *Chaetoceros* resting spores predominantly occur in high biogenic opal and TOC intervals (Fig. 4) and are commonly interpreted as indicating high primary production resulting from surface water stratification due to melt water (Leventer, 1991; Stockwell, 1991; Leventer et al., 1996; Sjunneskog and Taylor, 2002; Crosta et al., 2005). Thus, the high surface water productivity and nutrient limitation during interglacial periods occurs under a more stratified open ocean. This is presented as a schematic paleoceanographic model for interglacial periods (Fig. 6).

Glacial periods are characterized by low biogenic opal concentration, low TOC concentration, low WC, low bulk $\delta^{15}N$, high MS, high grain density, and high C/N ratio, and coarse MGS with abundant coarse grains (Fig. 3). The glacial characteristics indicate 1) low surface water productivity with low nitrate utilization; and 2) siliclastic influence derived from a glacimarine source. The dominant diatom species during glacial periods are sea ice related species and cold-water species, including *E. antarctica* var. *recta* (Fig. 4). Prothro et al. (2018) reported that calcareous foraminifera specimens dominate in an ice-proximal environment, which is consistent with previous observations that the abundance of *N. pachyderma* (sin.) in Antarctic continental shelves can be used as a proxy for ice shelf calving and the melting of ice masses close to ice marginal zones (Kellogg and Kellogg, 1988; Anderson et al., 1991). Previous studies found that a high abundance of N. *pachyderma* (sin.) occurred during the Last Glacial Maximum, and they linked this finding to the increased presence of sea ice (Bonaccori

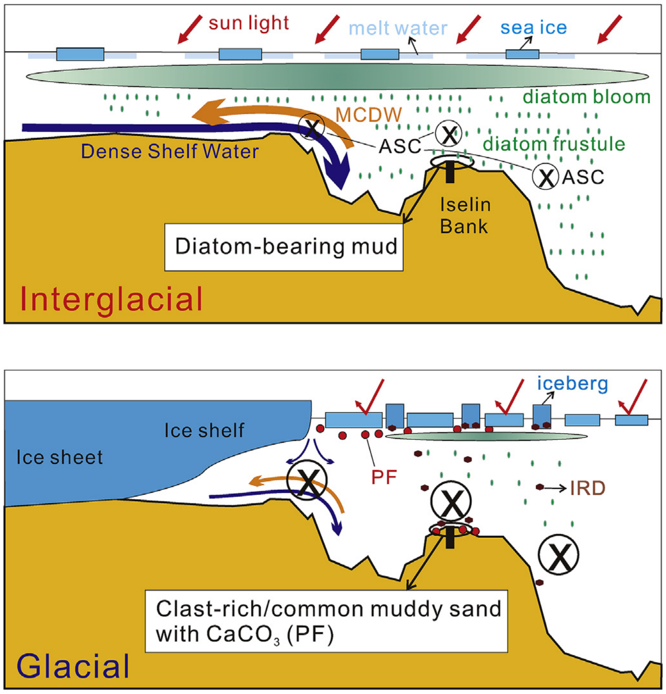

Fig. 6. Schematic models of the glacial periods and interglacial periods in the Iselin Bank region over the last 400 kyrs. The transect is shown in Fig. 1 as red line. Modified Circumpolar Deep Water (MCDW), Antarctic Slope Current (ASC), ice rafted debris (IRD), and planktonic foraminifer (PF).

and Melis, 2001). In addition, Asioli and Langone (1997) suggested that the occurrence of *N. pachyderma* (sin.) is related to annual sea ice conditions, and abundant living *N. pachyderma* (sin.) were found in sea ice in the Ross and Weddell Seas (Sprindler and Diekman, 1986; Diekmann et al., 1991; Quaia and Cespuglio, 2000). Thus, glacial sediments in the Iselin Bank area are deposited under cold and extensive sea ice conditions in close proximity to ice shelves or grounded ice sheet margins providing meltwater. Chase et al. (2015) reported that biogenic opal concentration and nutrient utilization decreases southward from the Antarctic Polar Front as sea ice duration increases. This is due to the light limitation resulting from the extensive sea ice cover, which restricts surface water productivity and decreases nitrate utilization during glacial periods in the Iselin Bank region. This result is supported by our observation of a high relative abundance of sea ice-related diatoms coinciding with low surface water productivity (Fig. 4).

In addition, higher C/N ratios indicate the relative increase in terrestrial input, which can decrease marine productivity and potentially increase glacimarine influence (and thus reworked terrestrial organic matter) due to the existence of more proximal ice masses. Abundant gravel grains, coarser MGS, skewness in grain size distributions, and coarse grain sizes indicate stronger bottom currents during glacial periods that restricted the deposition of fine grain clay. Given that this site is currently predominately influenced by zonal wind-driven ASC flows (Smith et al., 2012), stronger currents may have occurred during glacial periods in these locations (Thompson et al., 2018 and references therein). This theory is also supported by previous observations that calcareous foraminifera specimens dominate in higher-energy current settings in the Ross Sea continental margin (Prothro et al., 2018). The glacial paleoceanographic conditions are presented in a schematic model (Fig. 6).

6.2. Variation in $CaCO_3$ in the Ross Sea and its implication for bottom water mass change during the late pleistocene

$CaCO_3$ peaks, mostly planktonic foraminifers, in RS15-GC40 and RS15-GC41 occurred mostly during glacial periods, and $CaCO_3$ was better preserved in RS15-GC40 (1083 m in water depth) than in RS15-GC41 (1557 m in water depth) due to the shallower water depth of RS15-GC40 (Fig. 3). This indicates that the water column in the Ross Sea became less corrosive during glacial periods, which was potentially due to the accumulation of siliceous detritus on the sea floor that facilitated the decay of organic matter and dissolution of calcareous foraminifers during interglacial periods (Kennett, 1968). Conversely, strong bottom currents during glacial periods for RS15-GC40 and RS15-GC41 raised the $CaCO_3$ preservation by restricting fine material deposition (Taviani et al., 1993; Anderson, 1999; Frank et al., 2014). This is supported by the fact that $CaCO_3$ increases only occur during intervals of low biogenic opal and TOC concentrations and with coarse MGSs (Fig. S1).

6.3. Implications of Antarctic Slope Currents variations during the late pleistocene

Intrusions of CDW into the Ross Sea continental shelf area are largely regulated by current speed at the continental shelf edge, providing heat and salinity which have implications for marine ice sheet mass balance and the formation of dense waters on the continental shelf (Jacobs et al., 1970; Orsi and Wiederwohl, 2009; Gordon, 2009; Jacobs et al., 2011; Pritchard et al., 2012). The continental shelf exposure to open ocean and floating ice shelves, is important for dense water formation in the Antarctic continental shelf (Yabuki et al., 2016). However, as the marine-based Antarctic ice sheet terminated near the continental shelf break in the Ross Sea, the size of the Ross ice shelf cavity was also greatly reduced during the last glacial period (Anderson et al., 2002; Halberstadt et al., 2016), and this likely resulted in less continental shelf dense water formation. Thus, the enhanced bottom current at the Iselin Bank is unlikely to be directly related to the cascading density flows of super-cooled, saline shelf waters. Carbonate organisms are often found with benthic carbonates in outer shelf regions where there is enriched nutrient delivery by impinging CDW (Elverhoi and Roaldset, 1983; Taviani et al., 1993; Anderson, 1999). However, because the dominant component of $CaCO_3$ in RS15-GC40 and RS15-GC41 is planktonic foraminifer, either surface water conditions allowed for the increased productivity of foraminifera, or there was less CDW influence. Because the ASC currently flows along the Iselin Bank (Smith et al., 2012, Fig. 1) and is wind-driven (Thompson et al., 2018), the winnowing is most likely related to the enhanced ASC strength under windier glacial conditions, which is evidenced by the EDC ice core dust record (Fig. 5; Jouzel et al., 2007). Thus, it is revealed that winnowing mechanisms are regulated by shifts in wind speeds that govern ASC flow in the Iselin Bank during glacial periods.

The Weddell Sea has a wide shelf area and is a major contributor to AABW formation, which plays an important role in the deposition of $CaCO_3$ (Berger, 1970). Anderson (1975) reported that $CaCO_3$ dissolution in the Weddell Sea is related to water mass, particularly saline shelf water. Considering the similarities between the Ross Sea and the Weddell Sea, dense shelf water in the Ross Sea is considered to be undersaturated with respect to $CaCO_3$. Thus, the improved preservation of $CaCO_3$ can be attributed to the weakened formation of dense shelf water in the Ross Sea. CDW intrusion was weakened due to 1) the reduced shelf dense water formation in the Ross Sea and 2) a strong ASC acting as a hydrographic barrier to prevent CDW intrusion. Excellent $CaCO_3$ preservation can occur due to reduced CO_2-rich CDW. Thus, we propose that the improved preservation of $CaCO_3$ in the Iselin Bank is due to a combination of the restriction of fine siliceous detritus inputs and reduced influence of both CDW and shelf dense water during glacial periods. The glacial-interglacial $CaCO_3$ variation is shown in the schematic model (Fig. 6). However, because of the complicated bathymetry in the Ross Sea, there are likely to regional oceanographic differences; thus, to understand the entire temporal $CaCO_3$ variation system of the Ross Sea, additional studies are required.

7. Conclusions

In this study, the concentrations of biogenic opal, $CaCO_3$, and TOC, and bulk nitrogen isotopes, physical properties, and diatom assemblages of RS15-GC40 and RS15-GC41 were measured to reconstruct glacial-interglacial paleoceanographic changes during the late Quaternary period in the Ross Sea, including changes in surface water productivity, nutrient utilization, and bottom water mass ventilation. The main findings of this study are as follows:

1. The sedimentation rates and sedimentary compositions of the two cores are strongly correlated with both surface and bottom oceanographic changes associated with ice sheet/shelf dynamics. In addition, paleoceanographic records in the Iselin Bank display cyclic variations consistent with orbital-scale variations observed in ice core and deep-sea benthic isotope records.
2. High surface water productivity with enhanced nutrient utilization occurred under open marine conditions during interglacial periods. The co-occurrence of *Chaetoceros* resting pores indicates nutrient limitation under stratified surface water conditions.
3. Low surface water productivity with incomplete nutrient utilization occurred under extensive sea ice/ice proximal conditions during glacial periods, implying that there was light limitation due to the sea ice.
4. Grain size and $CaCO_3$ records indicate strong bottom currents during glacial periods that prevented the deposition of fine sediment and diatom frustules (winnowing). The intensified bottom currents during glacial periods were interpreted to be induced by wind-driven ASC.
5. $CaCO_3$ (mainly planktonic foraminifers) preservation in the Iselin Bank improved during glacial periods due to 1) the strong bottom current causing less organic matter decomposition by sweeping away fine materials and 2) the influence of grounded ice sheets on the continental shelf restricting the formation of corrosive dense shelf water that was undersaturated with respect to $CaCO_3$.

Declaration of competing interest

The authors declare that they have no known competing financial interests or personal relationships that could have appeared to influence the work reported in this paper.

Acknowledgements

We would like to thank the crew and scientific party of the IBR/V *Araon* for their support during the onboard gravity coring on board. We would like to thank the KOPRI laboratory members for their assistance with experimental measurements. We appreciate the handling editor (Dr. Ingrid Hendy) and two anonymous reviewers for their important and constructive comments to improve data interpretation and manuscript structure. This research was supported by KOPRI project (PE20180). Tis study was carried out by the National Research Foundation of Korea (Korea-Italy Joint Research Program; 2019K1A3A1A25000116).

Appendix A. Supplementary data

Supplementary data to this article can be found online at https://doi.org/10.1016/j.quascirev.2020.106356.

References

Ainley, D.G., Jacobs, S.S., 1981. Sea-bird affinities for ocean and ice boundaries in the Antarctic. Deep-Sea Res. Part A Oceanogr. Res. Pap. 28, 1173–1185. https://doi.org/10.1016/0198-0149(81)90054-6.

Anderson, J.B., 1975. Factors controlling $CaCO_3$ dissolution in the Weddell Sea from foraminiferal distribution patterns. Mar. Geol. 19, 315–332.

Anderson, J.B., 1999. Antarctic Marine Geology. Cambridge University Press, Cambridge.

Anderson, J.B., Kennedy, D.S., Smith, M.J., Domack, E.W., 1991. Sedimentary facies associated with Antarctica's floating ice masses. In: Anderson, J.B., Ashlye, G.M. (Eds.), Glacial Marine Sedimentation; Paleoclimatic Significance. Boulder, Colorado, GSA Special Paper 261.

Anderson, J.B., Shipp, S.S., Lowe, A.L., Wellner, J.S., Mosola, A.B., 2002. The antarctic ice sheet during the last glacial maximum and its subsequent retreat history: a review. Quat. Sci. Rev. 21, 49–70.

Anderson, J.B., Conway, H., Bart, P.J., Witus, A.E., Greenwood, S.L., McKay, R.M., Hall, B.L., Ackert, R.P., Licht, K., Jakobsson, M., Stone, J.O., 2014. Ross Sea paleo-ice sheet drainage and deglacial history during and since the LGM. Quat. Sci. Rev. 100, 31–54.

Anderson, J.B., Simkins, L.M., Bart, P.J., De Santis, L., Halberstadt, A.R.W., Olivo, E., Greenwood, S.L., 2019. Seismic and geomorphic records of Antarctic Ice Sheet evolution in the Ross Sea controlling factors in its behavior. Geol. Soc. London. Spec. Publ. 475, 223–240. https://doi.org/10.1144/SP475.5.

Armand, L.K., Crosta, X., Romero, O., Pichon, J.J., 2005. The biogeography of major diatom taxa in Southern Ocean sediments: 1. Sea ice related species. Palaeogeogr. Palaeoclimatol. Palaeoecol. 223, 93–126.

Arrigo, K.R., van Dijken, G.L., 2004. Annual changes in sea-ice, chlorophyll a, and primary production in the Ross Sea, Antarctica. Deep-Sea Res. II 51, 117–138.

Asioli, A., Langone, L., 1997. Relationship between recent planktonic foraminifera and water mass properties in the western Ross Sea (Antarctica). Geogr. Fis. Din. Quaternaria 20, 193–198.

Bak, Y.-S., Yoo, K.-C., Yoon, H.I., Lee, J.-D., Yun, H., 2007. Diatom evidence for Holocene paleoclimatic change in the South scotia sea, west Antarctica. Geosci. J. 11, 11–22.

Bart, P.J., Sjunneskog, C., Chow, J.M., 2011. Piston-core based biostratigraphic constraints on Pleistocene oscillations of the west antarctic ice sheet in western Ross Sea between north basin and AND-1B drill site. Mar. Geol. 289, 86–99. https://doi.org/10.1016/j.margeo.2011.09.005.

The RAISED Consortium, Bentley, M.J., Cofaigh, C.Ó., Anderson, J.B., Conway, H., Davies, B., Graham, A.G.C., Hillenbrand, C.-D., Hodgson, D.A., Jamieson, S.S.R., Larter, R.D., Mackintosh, A., Smith, J.A., Verleyen, E., Ackert, R.P., Bart, P.J., Berg, S., Brunstein, D., Canals, M., Colhoun, E.A., Crosta, X., Dickens, W.A., Domack, E., Dowdeswell, J.A., Dunbar, R., Ehrmann, W., Evans, J., Favier, V., Fink, D., Fogwill, C.J., Glasser, N.F., Gohl, K., Golledge, N.R., Goodwin, I., Gore, D.B., Greenwood, S.L., Hall, B.L., Hall, K., Hedding, D.W., Hein, A.S., Hocking, E.P., Jakobsson, M., Johnson, J.S., Jomelli, V., Jones, R.S., Klages, J.P., Kristoffersen, Y., Kuhn, G., Leventer, A., Licht, K., Lilly, K., Lindow, J., Livingstone, S.J., Massé, G., McGlone, M.S., McKay, R.M., Melles, M., Miura, H., Mulvaney, R., Nel, W., Nitsche, F.O., O'Brien, P.E., Post, A.L., Roberts, S.J., Saunders, K.M., Selkirk, P.M., Simms, A.R., Spiegel, C., Stolldorf, T.D., Sugden, D.E., van der Putten, N., van Ommen, T., Verfaillie, D., Vyverman, W., Wagner, B., White, D.A., Witus, A.E., Zwartz, D., 2014. A community-based geological reconstruction of antarctic ice sheet deglaciation since the last glacial maximum. Quat. Sci. Rev. 100, 1–9. https://doi.org/10.1016/j.quascirev.2014.06.025.

Berger, W.H., 1970. Biogenous deep-sea sediments: fractionation by deep-sea circulation. Geol. Soc. Am. Bull. 81, 1385–1402.

Bintanja, R., van de Wal, R.S.W., Oerlemans, J., 2005. Modelled atmospheric temperatures and global sea levels over the past million years. Nature 437, 125–128.

Bonaccorsi, R., Melis, R., 2001. Persistence of living planktonic foraminifera (*Neogloboquadrina pachyderma*) in Antarctic sea-ice inferred from a study of a sediment core (Ross Sea continental margin). In: Chela-Flores, J., Owen, T., Raulin, F. (Eds.), First Steps in the Orgin of Life in the Universe. Springer, Dordrecht, pp. 255–260.

Ceccarori, L., Frank, M., Frignani, M., Langone, L., Ravaioli, M., Mangini, A., 1998. Late Quaternary fluctuations of biogenic component fluxes on the continental slope of the Ross Sea, Antarctica. J. Mar. Syst. 17, 515–525.

Chase, Z., Kohfeld, K.E., Matsumoto, K., 2015. Controls on biogenic silica burial in the Southern Ocean. Global Biogeochm. Cycles 29, 1599–1616. https://doi.org/10.1002/2015GB005186.

Christ, A.J., Talaia-Murray, M., Elking, N., Domack, E.W., Leventer, A., Lavoie, C., Brachfeld, S., Yoo, K.-C., Gilbert, R., Jeong, S.-M., Petrushak, S., Wellner, J., the LARISSA Group, 2015. Late Holocene glacial advance and ice shelf growth in barilari bay, graham land, West Antarctic peninsula. Geol. Soc. Am. Bull. 127,

29–315. https://doi.org/10.1130/B31035.1.
Clark, P.U., Dyke, A.S., Shakun, J.D., Carlson, A.E., Clark, J., Wohlfarth, B., Mitrovica, J.X., Hostetler, S.W., McCabe, A.M., 2009. The last glacial maximum. Science 325, 710–714. https://doi.org/10.1126/science.1172873.
Collier, R., Dymond, J., Honjo, S., Manganini, S., Francois, R., Dunbar, R., 2000. The vertical flux of biogenic and lithogenic material in the Ross Sea: moored sediment trap observations 1996–1998. Deep-Sea Res. II 47, 3491–3520.
Crosta, X., Romero, O., Armand, L.K., Pichon, J.J., 2005. The biogeography of major diatom taxa in Southern Ocean sediments: 2. Open ocean related species. Palaeogeogr. Palaeoclimatol. Palaeoecol. 223, 66–92.
Cunningham, W.L., Leventer, A., Andrews, J.T., Jennings, A.E., Licht, K.L., 1999. Late Pleistocene-Holocene marine conditions in the Ross Sea, Antarctica: evidence from the diatom record. Holocene 9, 129–139.
DeMaster, D.J., 1981. The supply and accumulation of silica in the marine environment. Geochem. Cosmochim. Acta 5, 1715–1732.
Diekmann, G.S., Spindler, M., Lange, M.A., Ackley, S.F., Eicken, H., 1991. Antarctic sea ice: a habitat for the foraminifer *Neogloboquadrina pachyderma*. J. Foraminifer. Res. 21, 182–189.
Dinniman, M.S., Klinck, J.M., Smith Jr., W.O., 2011. A model study of circumpolar deep water on the west antarctic peninsula and Ross Sea continental shelves. Deep-Sea Res. II 58, 1508–1523.
Domack, E.W., 1992. Modern carbon-14 ages and reservoir corrections for the Antarctic Peninsula and Gerlache Strait area. Antarct. J. U. S. 27, 63–64.
Domack, E.W., Jacobson, E.A., Shipp, S., Anderson, J.B., 1999. Late pleistocene-holocene retreat of the west antarctic ice-sheet system in the Ross Sea: Part 2–sedimentologic and stratigraphic signature. Geol. Soc. Am. Bull. 111, 1517–1536.
Domack, E.W., Leventer, A., Dunbar, R., Taylor, F., Brachfeld, S., Sjunneskog, C., Cowan, E., Daniels, J.W., Escutia, C., Evans, A., Eyles, N., Guyodo, Y., Ioio, M., Iwai, M., Kyte, F., Lauer, C., Maldonado, A., Morez, T., Osterman, L., Pudsey, C., Schuffert, J., Vigar, K., Weinheimer, A., Williams, T., Winter, D., Wolf-Welling, T.C.W., 2001. Chronology of the palmer deep site, antarctic peninsula: a Holocene palaeoenvironmental reference for the circum-Antarctic. Holocene 11, 1–9. https://doi.org/10.1191/095968301673881493.
Elderfield, H., Ferretti, P., Greaves, M., Crowhurst, S., McCave, I.N., Hodell, D., Piotrowski, A.M., 2012. Evolution of ocean temperature and ice volume through the mid-Pleistocene climate transition. Science 337, 704–709.
Elverhoi, A., Roaldset, E., 1983. Glaciomarine sediments and suspended particulate matter, Weddell Sea shelf, Antarctica. Polar Res. 1, 1–21.
Folk, R.L., Ward, W.C., 1957. Brazos River bar [Texax]; a study in the significance of grain size parameters. J. Sediment. Res. 27, 3–26.
Frank, T.D., James, N.P., Bone, Y., Malcolm, I., Bobak, L.E., 2014. Late Quaternary carbonate deposition at the bottom of the world. Sediment. Geol. 305, 1–16. https://doi.org/10.1016/j.sedgeo.2014.02.008.
Gordon, A.L., 2009. Bottom water formation. In: Steele, J.H., Thorpe, S.A., Turekian, K.K. (Eds.), Ocean Currents. Associated Press, pp. 263–269.
Halberstadt, A.R.W., Simkins, L.M., Greenwood, S.L., Anderson, J.B., 2016. Past ice-sheet behavior: retreat scenarios and changing controls in the Ross Sea, Antarctica. Cryosphere 10, 1003–1020. https://doi.org/10.5194/tc-10-1003-2016.
Hillenbrand, C.D., Kuhn, G., Frederichs, T., 2009. Record of a Mid-Pleistocene depositional anomaly in West Antarctic Continental margin sediments: an indicator for ice-sheet collapse? Quat. Sci. Rev. 28, 1147–1159.
Hillenbrand, C.D., Larter, R.D., Dowdeswell, J.A., Ehrmann, W., Cofaigh, C.Ó., Benetti, S., Graham, A.G.C., Grobe, H., 2010. The sedimentary legacy of a palaeo-ice stream on the shelf of the southern Bellingshausen Sea: clues to West Antarctic glacial history during the Late Quaternary. Quat. Sci. Rev. 29, 2741–2763.
Hodell, D.A., Venz-Curtis, K.A., 2006. Late neogene history of deepwater ventilation in the Southern Ocean. Geochem. Geophys. Geosyst. 7, Q09001. https://doi.org/10.1029/2005GC001211.
Jacobs, S.S., Amos, A.F., Bruchhausen, P.M., 1970. Ross Sea Oceanography and Antarctic Bottom Water formation. Deep-Sea Res. 17, 935–962.
Jacobs, S.S., Jenkins, A., Giulivi, C.F., Dutrieux, P., 2011. Stronger ocean circulation and increased melting under Pine Island Glacier ice shelf. Nat. Geosci. 4, 519–523. https://doi.org/10.1038/ngeo1188.
Jouzel, J., Masson-Delmotte, V., Cattani, O., Dreyfus, G., Falourd, S., Hoffmann, G., Minster, B., Nouet, J., Barnoloa, J.M., Chappellaz, J., Fischer, H., Gallet, J.C., Johnsen, S., Leuenberger, M., Loulergue, L., Luethi, D., Oerter, H., Parrenin, F., Raisbeck, G., Raynaud, D., Schilt, A., Schwander, J., Selmo, E., Souchez, R., Spahni, R., Stauffer, B., Steffensen, J.P., Stenni, B., Stocker, T.F., Tison, J.L., Werner, M., Wolff, E.W., 2007. Orbital and millennial Antarctic climate variability over the past 800,000 years. Science 317, 793–796.
Kellogg, T.B., Kellogg, D.E., 1988. Antarctic cryogenic sediments: biotic and inorganic facies of ice shelf and marine-based ice sheet environments. Palaeogeogr. Palaeoclimatol. Palaeoecol. 67, 51–74.
Kennett, J.P., 1968. The fauna of the Ross Sea: part 6: ecology and distribution of foraminifera. Dept. Sci. Ind. Res. Bull. 186, 1–47.
Kim, S., Yoo, K.C., Lee, J.I., Khim, B.K., Bak, Y.S., Lee, M.K., Lee, J., Domack, E.W., Christ, A.J., Yoon, H.I., 2018. Holocene paleoceanography of Bigo Bay, west Antarctic Peninsula: connections between surface water productivity and nutrient utilization and its implication for surface-deep water mass exchange. Quat. Sci. Rev. 192, 59–70. https://doi.org/10.1016/j.quascirev.2018.05.028.
Lamb, A.L., Wilson, G.P., Leng, M.J., 2006. A review of coastal palaeoclimate and relative sea-level reconstructions using $\delta^{13}C$ and C/N ratios in organic material. Earth Sci. Rev. 75, 29–57.
Leventer, A., 1991. Sediment trap diatom assemblages from the northern Antarctic Peninsula region. Deep Sea Res. 38, 1127–1143.
Leventer, A., Dunbar, R.B., 1988. Recent diatom record of McMurdo Sound, Antarctica: implications for the history of sea-ice extent. Paleoceanography 3, 259–274.
Leventer, A., Domack, E.W., Ishman, S.E., Brachfeld, S., McClennen, C.E., Manley, P.L., 1996. Productivity cycles of 200–300 years in the Antarctic Peninsula region: understanding likages among the sun, atmosphere, oceans, sea ice, and biota. Geol. Soc. Am. Bull. 108, 1626–1644. https://doi.org/10.1130/0016-7606(1996)108<1626:PCOYIT>2.3.CO;2.
Leventer, A., Domack, E.W., Barkoukis, A., McAndrews, B., Murray, J., 2002. Laminations from the palmer deep: a diatom-based interpretation. Paleoceanography 17, 8002. https://doi.org/10.1029/2001PA000624.
Licht, K.J., Jennings, A.E., Andrews, J.T., Williams, K.M., 1996. Chronology of late Wisconsin ice retreat from the western Ross Sea, Antarctica. Geology 24, 223–226.
Licht, K.J., Dunbar, N.W., Andrews, J.T., Jennings, A.E., 1999. Distinguishing subglacial till and glacial marine diamictons in the western Ross Sea, Antarctica: implications for a last glacial maximum grounding line. GSA Bulletin 111, 91–103.
Lisiecki, L.E., Raymo, M.E., 2005. A Pliocene-Pleistocene stack of 57 globally distributed benthic $\delta^{18}O$ records. Paleoceanography 20, PA1003, 1029/2004PA001071.
Lüthi, D., Le Floch, M., Bereiter, B., Blunier, T., Barnola, J.M., Siegenthaler, U., Raynaud, D., Jouzel, J., Fischer, H., Kawamura, K., Stocker, T.F., 2008. High-resolution carbon dioxide concentration record 650,000–800,000 years before present. Nature 453, 379–382.
McGlannan, A.J., Bart, P.J., Chow, J.M., DeCesare, M., 2017. On the influence of post-LGM ice shelf loss and grounding zone sedimentation on West Antarctic ice sheet stability. Mar. Geol. 392, 151–169. https://doi.org/10.1016/j.margeo.2017.08.005.
McKay, R.M., Dunbar, G.B., Naish, T.R., Barrett, P.J., Carter, L., Harper, M., 2008. Retreat history of the Ross ice sheet (shelf) since the last glacial maximum from deep-basin sediment cores around Ross island. Palaeogeogr. Palaeoclimatol. Palaeoecol. 260, 245–261. https://doi.org/10.1016/j.palaeo.2007.08.015.
McKay, R., Browne, G., Carter, L., Cowan, E., Dunbar, G., Krissek, L., Naish, T., Powell, R., Reed, J., Talarico, F., Wilch, T., 2009. The stratigraphic signature of the late cenozoic antarctic ice sheets in the Ross embayment. GSA Bulletin 121, 1537–1561. https://doi.org/10.1130/B26540.1.
McKay, R., Naish, T., Carter, L., Riesselman, C., Dunbar, R., Sjunneskog, C., Winter, D., Saniorgi, F., Warren, C., Pagani, M., Schouten, S., Willmott, V., Levy, R., DeConto, R., Powell, R.D., 2012. Antarctic and Southern Ocean influences on late pliocene global cooling. Proc. Natl. Acad. Sci. Unit. States Am. 109, 6423–6428. https://doi.org/10.1073/pnas.1112248109.
McKay, R., Golledge, N.R., Maas, S., Naish, T., Levy, R., Dunbar, G., Kuhn, G., 2016. Antarctic marine ice-sheet retreat in the Ross Sea during the early Holocene. Geology 44, 7–10. https://doi.org/10.1130/G37315.1.
McKay, R.M., De Santis, L., Kulhanek, D.K., the Expedition 374 Scientists, 2019. Ross Sea West Antarctic ice sheet history. In: Proceedings of the International Ocean Discovery Program, 374: College Station, TX (International Ocean Discovery Program). https://doi.org/10.14379/iodp.proc.374.2019.
Mortlock, R.A., Froelich, P.N., 1989. A simple method for the rapid determination of opal in pelagic marine sediments. Deep-Sea Res. 36, 1415–1426.
Naish, T., Powell, R., Levy, R., Wilson, G., Scherer, R., Talarico, F., Krissek, L., Niessen, F., Pompilio, M., Wilson, T., Carter, L., DeConto, R., Huybers, P., McKay, R., Pollard, D., Ross, J., Winter, D., Barrett, P., Browne, G., Cody, R., Cowan, E., Crampton, J., Dunbar, G., Dunbar, N., Florindo, F., Gebhardt, C., Graham, I., Hannah, M., Hansaraj, D., Harwood, D., Helling, D., Henrys, S., Hinnov, L., Kuhn, G., Kyle, P., Läufer, A., Maffioli, P., Magens, D., Mandernack, K., McIntosh, W., Millan, C., Morin, R., Ohneiser, C., Paulsen, T., Persico, D., Raine, I., Reed, J., Riesselman, C., Sagnotti, L., Schmitt, D., Sjunneskog, C., Strong, P., Taviani, M., Vogel, S., Wilch, T., Williams, T., 2009. Obliquity-paced pliocene West Antarctic ice sheet oscillations. Nature 458, 322–328. https://doi.org/10.1038/nature07867.
NSIDC, 1998. Distributed Active Archive Center. NSIDC. http://www-nsidc.colorado.edu/NSIDC/CATALOG/ENTRIES/nsi-0056.html.
Orsi, A.H., Wiederwohl, C.L., 2009. A recount of Ross Sea waters. Deep-Sea Res. II 56, 778–795.
Paillard, D., Laeyrie, L., Yiou, P., 1996. Macintosh Program Performs Time-Series Analysis, vol. 77. EOS Transactions American Geophysical Union, Washington D.C., p. 379
Pritchard, H.D., Ligtenberg, S.R.M., Fricker, H.A., Vaughan, D.G., Broeke, M.R. van den, Padman, L., 2012. Antarctic ice sheet loss driven by basal melting of ice shelves. Nature 484, 502–505. https://doi.org/10.1038/nature10968.
Prothro, L.O., Simkins, L.M., Majewski, W., Anderson, J.B., 2018. Glacial retreat patterns and processes determined from integrated sedimentology and geomorphology records. Mar. Geol. 395, 104–119. https://doi.org/10.1016/j.margeo.2017.09.012.
Quaia, T., Cespuglio, G., 2000. Stable isotopes records from the western Ross Sea continental slope (Antarctica): considerations on carbonate preservation. Terra Antarctica Rep. 4, 199–210.
Reimer, P.J., Bard, E., Bayliss, A., Beck, J.W., Blackwell, P.G., Ramsey, C.B., Buck, C.E., Cheng, H., Edwards, R.L., Friedrich, M., Grootes, P.M., Guilderson, T.P., Haflidason, H., Hajdas, I., Hatté, C., Heaton, T.J., Hoffmann, D.L., Hogg, A.G., Hughen, K.A., Kaiser, K.F., Kromer, B., Manning, S.W., Niu, M., Reimer, R.W.,

Richards, D.A., Scott, E.M., Southon, J.R., Staff, R.A., Turney, C.S.M., van der Plicht, J., 2013. IntCal13 and Marine13 Radiocarbon age calibration curves 0-50,000 years cal BP. Radiocarbon 55, 1869–1887.

Robinson, R.S., Brzezinski, M.A., Beucher, C.P., Horn, M.G.S., Bedsole, P., 2014. The changing roles of iron and vertical mixing in regulating nitrogen and silicon cycling in the Southern Ocean over the last glacial cycle. Paleoceanograhpy 29, 1179–1195. https://doi.org/10.1002/2014PA002686.

Scherer, R.P., 1994. A new method for the determination of absolute abundance of diatoms and other silt-sized sedimentary particles. J. Paleolimnol. 12, 171–180.

Siddall, M., Hönisch, B., WaelBroeck, C., Huybers, P., 2010. Changes in deep pacific temperature during the mid-pleistocene transition and quaternary. Quat. Sci. Rev. 29, 170–181.

Simkins, L.M., Anderson, J.B., Greenwood, S.L., Gonnermann, H.M., Prothro, L.O., Halberstadt, A.R.W., Strearns, L.A., Pollard, D., DeConto, R.M., 2017. Anatomy of a meltwater drainage system beneath the ancestral East Antarctic ice sheet. Nat. Geosci. 10, 691–697. https://doi.org/10.1038/NGEO3012.

Sjunneskog, C., Taylor, F., 2002. Postglacial marine diatom record of the palmer deep, antarctic peninsula (ODP leg 178, site 1098) 1. Total diatom abundance. Paleoceanography 17. https://doi.org/10.1029/2000PA000563.

Smith, W., Sedwick, P., Arrigo, K., Ainley, D., Orsi, A., 2012. The Ross Sea in a sea of change. Oceanography 25, 90–103. https://doi.org/10.5670/oceanog.2012.80.

Sprenk, D., Weber, M.E., Kuhn, G., Rosén, P., Frank, M., Molina-Kescher, M., Liebetrau, V., Röhling, H.G., 2013. Southern Ocean bioproductivity during the last glacial cycle- new detection method and decadal-scale insight from the Scotia Sea. Geol. Soc. London Spec. Publ. 381, 245–261. https://doi.org/10.1144/SP381.17.

Sprindler, M., Dieckman, G.S., 1986. Distribution and abundance of the planktonic foraminifer Neogloboquadrina pachyderma in sea ice of the Weddell Sea (Antarctica). Polar Biol. 5, 185–191.

Stockwell, D.A., 1991. Distribution of *Chaetoceros* resting spores in the quaternary sediments from leg 119. In: Barron, J., Larsen, B., et al. (Eds.), Proc. ODP, Sci. Res., vol. 119. Ocean Drilling Program), College Station, TX, pp. 599–610.

Stuiver, M., Reimer, P.J., 1993. Extended 14C database and revised CALIB radiocarbon calibration program. Radiocarbon 35, 215–230.

Taviani, M., Reid, D.E., Anderson, J.B., 1993. Skeletal and isotopic composition and paleoclimatic significance of late Pleistocene carbonates, Ross Sea, Antarctica. J. Sediment. Res. 63, 84–90.

Thompson, A.F., Stewart, A.L., Spence, P., Heywood, K.J., 2018. The antarctic slope current in a changing climate. Rev. Geophys. 56, 741–770. https://doi.org/10.1029/2018RG000624.

Wu, L., Wang, R., Xiao, W., Ge, S., Chen, Z., Krijgsman, W., 2017. Productivity-climate coupling recorded in Pleistocene sediments off prydz bay (East Antarctica). Palaeogeogr. Palaeoclimatol. Palaeoecol. 485, 260–270. https://doi.org/10.1016/j.palaeo.2017.06.018.

Yabuki, T., Suga, T., Hanawa, K., Matsuoka, K., Kiwada, H., Watanabe, T., 2006. Possible source of the Antarctic bottom water in the Prydz Bay region. J. Oceanogr. 62, 649–655. https://doi.org/10.1007/s10872-006-0083-1.

Yoon, H.I., Yoo, K.C., Bak, Y.S., Lee, Y.I., Lee, J.I., 2009. Core-based reconstruction of paleoenvironmental conditions in the southern Drake Passage (West Antarctica) over the last 150 ka. Geo Mar. Lett. 29, 309–320. https://doi.org/10.1007/s00367-009-0144-8.